Hydrogeological monitoring and image analysis of a mudslide in Southern Italy

M. Polemio(1) and O. Petrucci(2)
(1) CNR-CERIST - Bari, Italy, m.polemio@ba.irpi.cnr.it
(2) CNR-IRPI - Rende, Italy

Abstract. This paper describes a methodological example of a data-integration procedure to improve the knowledge of landslide hazard related to a seismic area in the southern Apennine (Italy). Attention is focused on remote sensing data. The analysis is validated using detailed topographical, geophysical, geotechnical and hydrogeological data as *ground truth*. The investigated phenomenon, which started at the end of 1993, is an earthflow. The presented methodology recommends the combined use of DEM, multi-temporal panchromatic visible aerial photographs and thermal infrared images. The integration between these data and multidisciplinary monitoring data proved useful. The main hydrogeological pattern, the geological and geomorphological framework and the areas of latent instability can be clearly determined. Insight can be gained through the synoptic slope view in the relative short time needed to carry out the analysis. The proposed approach can be regarded as a useful contribution to the evaluation of landslide hazard, particularly during emergency periods.

1. Introduction

The study area is located in the Sele River basin (Fig.1), a tectonically active valley bordered by carbonate massifs. The area has been shaped by the Apennine tectonics beginning in the Middle-Upper Miocene and still active throughout the Plio-Pleistocene. The morpho-structural setting has been mainly formed during the last Lower Pliocene-Quaternary events (Agnesi et al., 1983).

Slope instability and floods have long been a constant feature in the area, often resulting in dreadful economic and human losses.

Four main landslides active during this century can be identified in the area. One of these phenomena has been analysed in detail in this paper. The phenomenon under study, which started in late 1993, is an earthflow that is in actual fact part of a larger landslide which was activated by the 1980 earthquake. Interdisciplinary investigations and monitoring were carried out between 1994 and 1996, within an EC funded research project (EC, 1996) and partially continued by Authors.

This area has been chosen as a case study owing both to the landslide dimensions, which are large enough to allow remote sensing, and the wealth of available data. The selection of the most suitable kind of data - mainly remotely sensed - and the proposal of the most appropriate processing is aimed at improving landslide knowledge. The availability of field data ensures the validation of the proposed work.

The combined analysis of DEM, panchromatic visible aerial photographs and thermal infrared images has been carried out aiming to perform a study approach able to provide a multi-temporal and multi-spectral analysis of slope instability phenomena. This framework has then been merged to data coming from multidisciplinary monitoring of study area in order to both verify the results of image analysis and test the proposed methodology.

Corrispondence to: Maurizio Polemio

2. Geological and hydrogeological setting

In the upper Sele River Valley four types of soils and rocks outcrop.

Limestone and *dolomitic limestone* which constitute the relief along the eastern and western edges of the Sele valley (Figs.1 and 2). The carbonate rocks make up the Polveracchio and Marzano mountains. The landscape is characterised by high-energy relief. As a result of the geotechnical characteristics of rocks, slopes are either steep or vertical. The rectangular pattern of the drainage network is mainly the result of the strong structural control (Fig.2). The rocks are liable to secondary mass movements, mostly rockfalls and topples.

A DEM (20 m *x* 20 m cell size), obtained by digitising official 1:25,000 scale maps, clearly shows carbonate rocks affected by a large D.G.P.V. (about 4.3 km in length and 4.1 km in width) in the Montenero Mt. area (Fig.1). This figure also highlights the control exerted by a set of WNW-

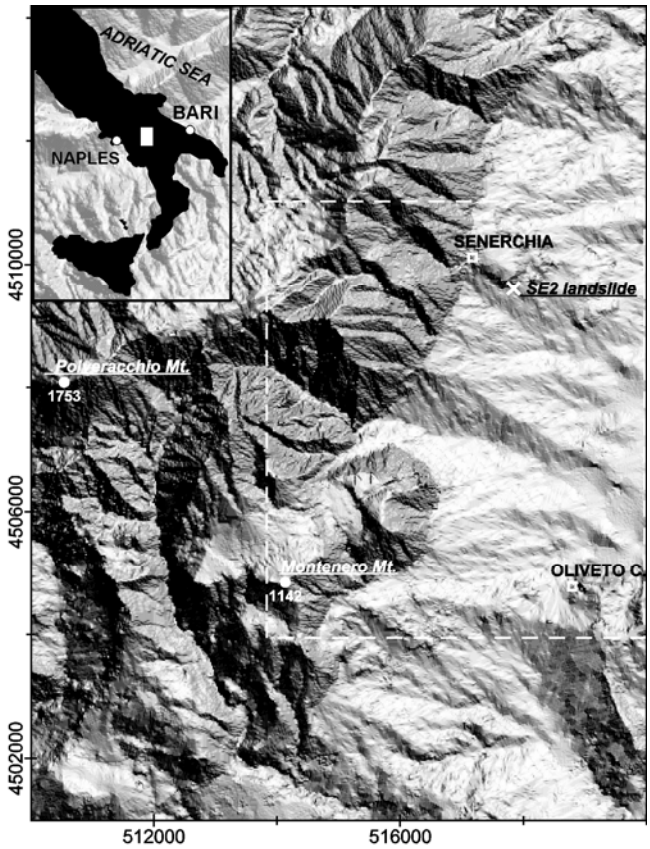

Fig.1. Twenty-meter resolution digital terrain model of the area represented as "real-time sun-shaded" image. The broken line is the Fig.3 boundary.

ESE-oriented tectonic discontinuities on the slope stability of the Senerchia area.

Carbonate rocks constitute a large aquifer, which is part of the Mts. Polveracchio-Raione hydrogeologic unit (Celico and Civita, 1976) and possess the highest relative permeability. The main springs (spring no. 1 and 2 in Fig.2, about 570 l/s in total) are located where the outcropping limit between the carbonate aquifer and the other lithotypes lies at the minimum elevation.

Varicoloured clays, in which the study area develops, are constituted by clayey-marly and clayey-marly-arenaceous flysch, shales, marls and chert limestones. They outcrop downslope the carbonate relief on both sides of the Sele valley (Fig.2). Clays show a marked heterogeneity and anisotropy tied to the geological and tectonic history. Tectonic events and mass movements are largely responsible for the remoulding of soils.

Clayey slopes are characterised by low-medium acclivity. The pattern of the drainage network is dendritic. Due to their mechanical and geotechnical behaviour, these sequences are extremely prone to creep and landslide phenomena. Complex and composite landslides, starting as rotational or translational slides and evolving downslope to flow, are widespread. The main scarps of the landslides are often located near the contact area between clays and carbonate rocks or detrital deposits. The clayey soils act as an impervious bounding for other lythotypes. When considered as a whole, at a synoptic scale, they show the minimum relative permeability. Hence, it is reasonable to assume that remoulding, locally and especially at shallow depths, increases hydraulic conductivity and porosity.

Detrital and *breccia deposits* are rockfall or scree of carbonate or piroclastic nature (Fig.2). They outcrop along a narrow strip located between the carbonate relief and clayey slopes. They also constitute a large debris slab in a limited quadrangular area (about 0.5 km^2), where the present town of Senerchia stands. It is a fan of 100 m maximum thickness that lies on clays (Guerricchio and Melidoro, 1981; Alexander and Coppola, 1989; Cotecchia, 1986) (Fig.2.). The slab lies in contact with the carbonate rocks to the west, and is threatened by the adjoining SE1 and SE2 landslides to the south and by the Pergola landslide to the east (Cotecchia et al., 1986).

Its relative permeability is medium to high. These deposits make up a secondary aquifer, which upslope is hydrogeologically in contact with the main aquifer. The detrital aquifer supplies the perennial spring no. 4, which is the nearest to the SE2 landslide.

Alluvial deposits, located along the Sele river bed and its main tributaries, have a middle relative permeability. They outcrop downslope landslide prone areas and are not relevant to the studied phenomena.

3. Recent landslides

Many ancient landslides have interested clayey terrain in the study area, but only four active landslides are known (Fig.2) during the last century.

The *SE1 landslide*, extending about 2500 m in length, 350 m in width and 30 m in depth (Cotecchia et al., 1986; Maugeri et al., 1982), is a complex landslide which started as a translational earth slide in the upper portion and evolved into a mudslide in the medium-lower sector. The main scarp is located near the contact area between clays and carbonate or detrital deposits. The landslide was activated in 1980, 15 hours after the last of the eleven strong earthquakes (*Msk intensity* VII or greater) which have hit Senerchia since 1400 (Alexander and Coppola, 1989). Because of the very low strength shown by clayey soils which constitute the landslide body, it has been generally regarded as a reactivated phenomenon (Cotecchia et al., 1986; Maugeri et al., 1982). On the other hand, the 1930 and 1962 earthquakes (IX÷X MSK intensity) are not known to have had any impact on it. Moreover, the 1955 aerial photos do not show any well-defined landslide body. Only in the lower landslide sector tracks of instability phenomena were recognisable (Maugeri et al., 1982). The earthquake disrupted an important aqueduct, which crossed the top of the landslide body, in the area where the SE1 movement started.

A hydrological-statistical approach has been carried out to understand the role of antecedent rainfall on the landslide activations, considering both the direct precipitation on landslide slopes and the recharge of carbonate aquifers (Polemio, 1997; Polemio and Dragone, 1998). The research has indicated the earthquake as the main triggering factor for the SE1 landslide, though prior to

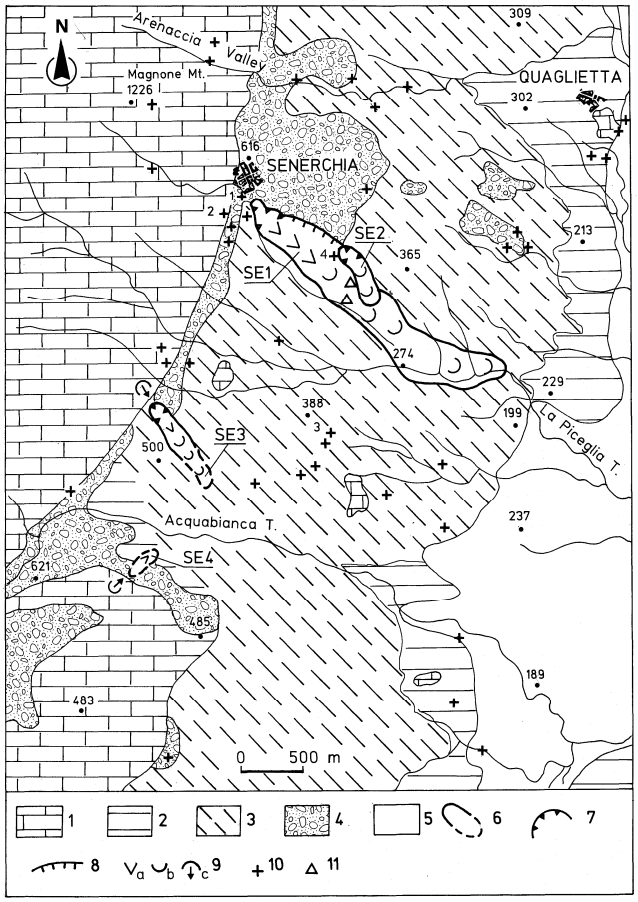

Fig.2. Geological and hydrogeological map of the study area. 1) limestone and dolomitic limestone, middle to very high relative secondary permeability; 2) Varicoloured clays, very low to low relative primary permeability; 3) like the previous one but remoulded by ancient or recent landsliding activity, middle secondary permeability of the shallow part; 4) detrital and breccia deposits, middle to high relative secondary permeability; 5) alluvial deposits, middle relative primary permeability; 6) boundary of landslide body, broken line where uncertain; 7) main scarp; 8) secondary landslide scarp; 9) rototraslational or traslational sliding (a), debris or earth flow (b), rockfall (c); 10) spring and its number if mentioned; 11) dried up spring.

the landslide activation heavy rainfall was observed in the recharge area of carbonate aquifers.

No significant earthquake and displacement have been seen to have taken place between 1980 and 1993 within or in the vicinity of the SE1 landslide (Del Gaudio et al., 1997).

The *SE2 landslide* is about 520 m in length and more than 10 m in depth; the main crown is 70 m large and the secondary left crown is 60-m large. The accumulation zone, after a 40-m large "bottleneck", spans across an area of about 135 m. The landslide is the enlargement of a subordinate slide situated on the left flank of the SE1 landslide. Since 1980 a slow retrogression of the rear scarp has taken place at the crown of the SE2 landslide. The reactivation of a lateral portion of the SE1 landslide was observed on December 29, 1993, with a wide retrogressive evolution.

The SE2 landslide gave rise to a rotational slide at the crown which then evolved downslope into an earthflow-mudslide. It is a composite phenomenon, which will be referred to as an earthflow (Cruden and Varnes, 1996), although its movement and type of deformation is halfway between that of a mudslide and that of an earthflow (Santaloia et al., in press). The SE2 toe is locally superimposed on the SE1 landslide body. This landslide, continuously surveyed since December 1994, is still active, though its activity has greatly decreased. Its ground surface inclination ranges from 10 to 15°; the main scarp is very steep (more than 45°).

The *SE3* and *SE4 landslides* occurred in Sierra Piano and Bosco, respectively in November and December 1996 (Polemio, 1997). The former is a mudslide (800 m in length, 70 m in width and less than 7 m in depth); the latter is a debris flow (250 m in length, 50 m in width and less than 6 m in depth).

The mean annual rainfall in Senerchia is 1600 mm and temperature is 12.8 °C. According to the Thornthwaite-Mather method (1957), evapotranspiration equals 570 mm. Therefore, 1030 mm are available for infiltration and runoff from November to May, which is the period of the year when the hydrogeological conditions are most prone to landsliding. The four aforementioned landslides occurred in November and December and, except for the SE1 landslide, all landslides were triggered during heavy rain periods in the Senerchia area. However, mean values can be misleading. The hydrological/statistical analysis of daily cumulative rainfall indicates that the reactivation of the SE2 landslide cannot be associated with rainfalls (Polemio, 1997). The concomitant rain can be viewed as an additional rather than a decisive factor, which has acted on pre-existing conditions of precarious stability. With a few differences, the analysis of the SE3 activation yields results similar to that of the SE2 landslide. A moderate influence of rain on landslide activation is observed only in the SE4 landslide.

Lacking any of the seismic action recorded in the SE1 case, the SE2-SE4 landslides are related to the evolution of the Sele Valley, which is still undergoing a complex dynamic process.

3.1 SE2 landslide investigation

Fifteen continuous coring boreholes, equipped with piezometers or inclinometers, were drilled to investigate the SE2 landslide (EC, 1996). Displacements at ground level were monitored through topographic and GPS surveying optimised by an aero-photogrammetric survey. Two climatic gauges and two accelerometers allowed climatic and seismic monitoring.

The geothecnical characterisation showed the poor shear strength of clayey soils, which did not improve with depth (Santaloia et al., in press).

The piezometric data logged at depth of more than 10 m were never affected by short-lasting and heavy rainfall events. By contrast, at shallower depths the piezometric response to rainfall was very quick (less than 20 hours to reach the maximum piezometric level after a rainfall event). The shallow clayey soil is located within the most disturbed section of the earthflow and constitutes a hydrogeological

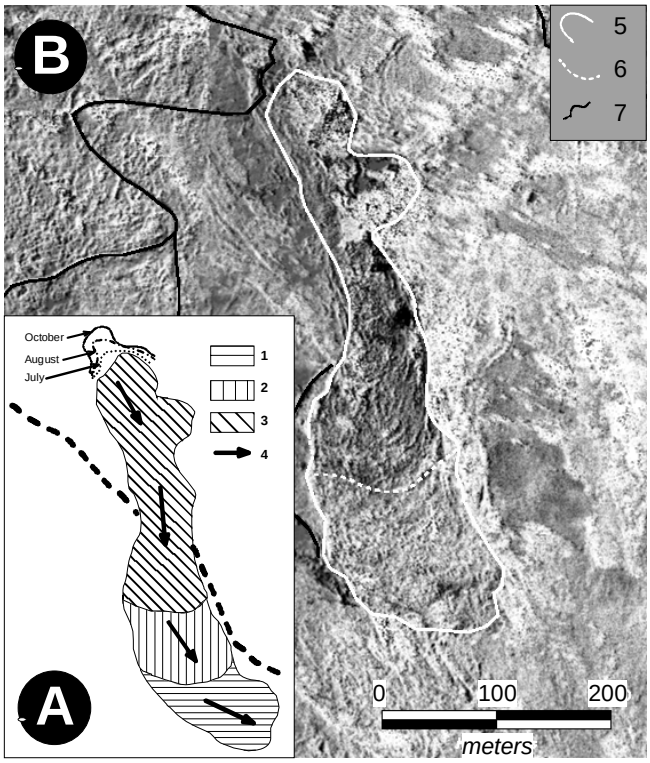

Fig.3. (A) SE2 Horizontal displacements from June 23, 1995 to October 14, 1995.Displacements rates (m/month): 1) 0.02÷0.2, 2) 0.4÷10 and 3) 10÷20; 4) main displacement direction. (B) Normalised difference ratios of SW and LW infra-red morning data. 5) SE2 landslide body; 6) separation line between different tone and texture areas; 7) main roads.

complex with higher void ratios and coefficient of permeability than deeper clayey soils.

The landslide body shows local acceleration. The maximum displacement rates were observed between May and October 1995. The highest movement velocity was observed along the channel (1.33 m/day, 72 m in 54 days). Fig.3A reports the movements between June 1995 (aerial photograph data) and October 1995 (infrared data).

The activity at the toe of the landslide was related to deep-seated active displacements (Santaloia et al., in press). The superficial displacements in 1995 were, at least in part, the result of short and heavy rainfall. The deep-seated displacements seem not to be directly related to these rainfall events.

The SE2 landslide resulted from an array of mechanisms of deformation and failure: a retrogressive slipping mechanism at the crown, an earthflow downslope and an underlying deep-seated mechanism of slow irreversible movements.

4. Data processing

In order to infer detailed data on the landslide area and its time/space evolution, a set of multi-spectral and multi-temporal data has been analysed with reference to the SE2 landslide. Multi-spectral data, particularly Infra-Red (IR) images have provided information otherwise inaccessible. The multi-temporal characteristic of the image data set has allowed observing the unstable area at different steps of its evolution and gain insight on its future development.

The analysed data-set includes: 1) a DEM (20 m *x* 20 m cell size) obtained by digitising official 1:25,000 scale maps derived from the 1955 aerial photography (Fig. 1); 2) 1980 panchromatic visible black and white aerial photographs (approx. scale 1:13,000); 3) 1995 panchromatic visible black and white aerial photos, at approx. 1:12,000 scale, covering also a wide area surrounding the unstable zone; 4) 1995 colour panchromatic visible aerial photos, at about 1:7,000 scale, of a narrow area around the SE2 landslide; 5) a topographic map, (1: 5,000 scale) in raster format, obtained from 1980 aerial photographs; 6) 1995 thermal infra-red images, gathered two times during the same day in two different bands (2-5 μm and 8-14 μm, *Short Wave Image* and *Long Wave Image* respectively, hereinafter *SWI* and *LWI*) from a flight elevation of 400 m. Each strip was about 320 m in width and had a geometric resolution of 1 m; 7) a DEM of the study area (1m *x* 1m cell size) and a topographic map (1: 2,000 scale) in vector format obtained from aerial photographs taken in June 1995.

4.1 Aerial photographs

All the available aerial photographs have been scanned and processed as raster files. In order to remove geometric and radiometric distortions and geo-referencing data to an Earth Coordinate System, the pre-processing operation of *geometric correction* has been carried out (Lillesand and Kiefer, 1994). The technique makes use of the coordinates of *ground control points* in a linear regression model to calculate a space transformation of data (Sabins, 1987). The aerial photographs have been geo-coded using an *image to image geo-correction* (AMS, 1999). The technique matches the coordinate systems of two digital images, one of which acting as a reference image and the other as the image to be rectified. In our case, all the aerial photographs have been geo-coded using the vector file of the topographic map (1: 2,000 scale) as the reference map. After the geo-coding procedure, the images of the same epoch have been used to obtain three different mosaics, representing the landscape framework in 1980 and 1995 respectively (in black and white and in colour).

A simple *linear contrast stretch* (Drury, 1987) and the cut-off of histogram tails have yielded a series of images which showed well-contrasted terrain details. For some aerial photographs high and low frequency *spatial filters* have also been used to emphasise directional and non directional differences in the spectral values summarised at some kernel dimension (Walsh et al., 1998).

The processed images have been used to obtained mosaics which emphasise changes in mass movement activity, enlargement of the involved area and land use pattern modifications by means of multi-temporal photo-interpretation.

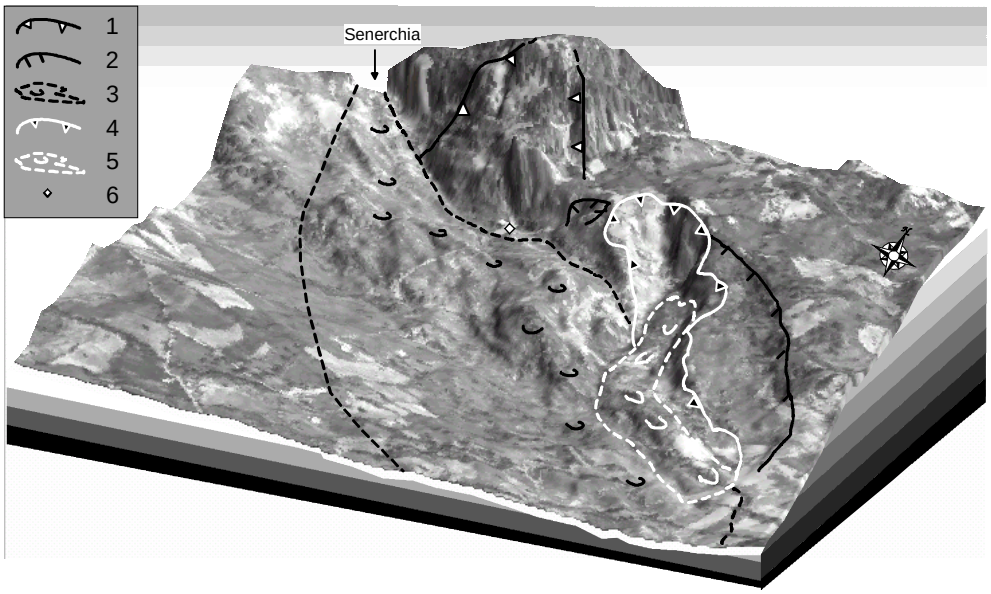

Fig.4. Three-dimensional view of the study zone (geometric resolution: 1 meter) obtained draping a mosaic of visible 1995 aerial photographs on a DEM of the area. 1) Ancient landslide, 2) relict of the SE1 landslide scarp, 3) SE1 landslide, 4) SE2 landslide crown, 5) spring n. 4 (see Fig.2).

4.2 Three-dimensional views

A DEM of the area, characterised by a geometric resolution of 1 meter, has been processed to obtain several three-dimensional sights of the unstable area. The possibility of modifying both the point of view and the vertical scale exaggeration has allowed obtaining several block-diagrams of the area highlighting the main tectonic features and morphological characteristics.

In order to improve the interpretation, an additional information layer, corresponding to the mosaic of the visible 1995 aerial photographs, has been draped on the 3-D views. The texture aerial photographs lying over the exaggerate relief model of the area allows a better definition of the geometrical elements. Fig.4 illustrates both the SE1 and SE2 landslides, and some evidences of an ancient landslide (Cotecchia et al., 1986). The illumination conditions help to easily trace both the crown walls of the SE2 landslide, marked by a white denudation zone, and the limits of its accumulation zone. This point of view is not sufficiently suitable to trace the right flank of the SE1 landslide which has been partially reshaped by natural erosion and human agency. Other block diagrams, obtained by rotating clock-wise the DEM, have been used to carry out this delimitation. Under different illumination conditions, the morphological discontinuity between the linear profile of the right flank of the valley and the convex one of the landslide body has been made evident.

4.3 Infra-red images

The Infra-Red region of the electromagnetic spectrum ranges in wavelength from 0.7 to 300 μm. The reflected IR region ranges from 0.7 to 3 μm. IR radiation at wavelength from 3 to 14 μm is called the thermal IR region. Exhaustive reviews on this topic can be found in specialised textbooks (Sabins, 1987; Drury, 1987). Unlike images of shorter wavelength radiation, the tone of a thermal image is tied to the surface temperature and not to the reflectance, since IR images detect the radiant energy emitted by the ground.
On images of the same area, taken at different times of the day, various signatures account for different materials and vegetation cover or for the same soil with different water contents.

There are two basic approaches to understand the significance of thermal IR images. The first uses complex mathematical models to relate surface temperature to the physical properties of materials. The second, which has been used in this work, makes an empirical correlation between the image signature and the corresponding soil features. Warm and cool areas in the image can be matched with different soils, water content, vegetation cover and soil morphology. Generally speaking, in grey scale representations, the brightest tones represent the warmest radiant temperature (that is the concentration of the radiant flux of a body) and the darkest tones represent the coolest temperature.

Thermal inertia of a surface is a measure of the resistance to temperature changes. It increases linearly with the increase in the density of the material. The difference between maximum and minimum temperature occurring during a day is called Δt. Soils with low thermal inertia (i.e. shale and volcanic cinders) have a low resistance to temperature changes and a relatively high Δt. They reach a high maximum surface temperature in the daytime and a low minimum temperature at night. Materials with high thermal inertia (sandstone and basalt) are relatively cool in the daytime and warm at night. Water bodies are cooler than soils in the daytime and warmer at night. Humid soil is cooler than dry soil, both during the day and at night.

Cross-track scanner systems, as the one used in this work, produce a typical geometric distortion characterised by an S-shaped curvature of straight elements that must be correct before arrange image in mosaics.

Images have been taken during October 1995, from a flight elevation of about 400 m, with a ground geometric resolution of 1 m. The analysed data-set consists of two couples of images: two morning images, taken one hour after the sunrise and relating to the 2-to-5μm band (*Ms* in the followings) and 8-to-14 μm (*Ml*), respectively; two afternoon images, taken one hour before the sunset and relating to the 2-to-5μm band (*As* in the followings) and 8-to-14 μm (*Al*), respectively.

The images have been merged to make four mosaics, which were then contrast enhanced. The results of this operation are shown in Fig.3. Topographic features are well defined in the morning images due to the insolation effect, which determines a differentiated thermal response of the morphological features. The overall radiant temperature level and the thermal contrasts among terrain features of the SWIs are otherwise lower than in the LWIs. Hence, LWIs are useful for terrain mapping, whereas SWIs are optimum for mapping hot targets, such as fires (Sabins, 1987) or many hand made subjects. These are the reasons why the Ml images have been used to identify geological and geomorphological lines, such as to trace the SE2 landslide body limits (white line in Fig.5).

The morning and afternoon images help emphasise different terrain features. During daylight hours images are affected by topography: the solar shadowing highlights the topography, areas in shadow are cool, and appear dark just like in conventional images. When approaching the sunset, the effect of the differential solar heating lasts for some time. In materials with the same thermal inertia, the hottest surfaces cool more quickly and topographic effects are gradually removed.

Hence, the Al and As images seem to be morphologically poorly detailed with respect to the Ml and Ms images (Fig.5). However, in the afternoon images darker areas can be considered as an expression of cool and

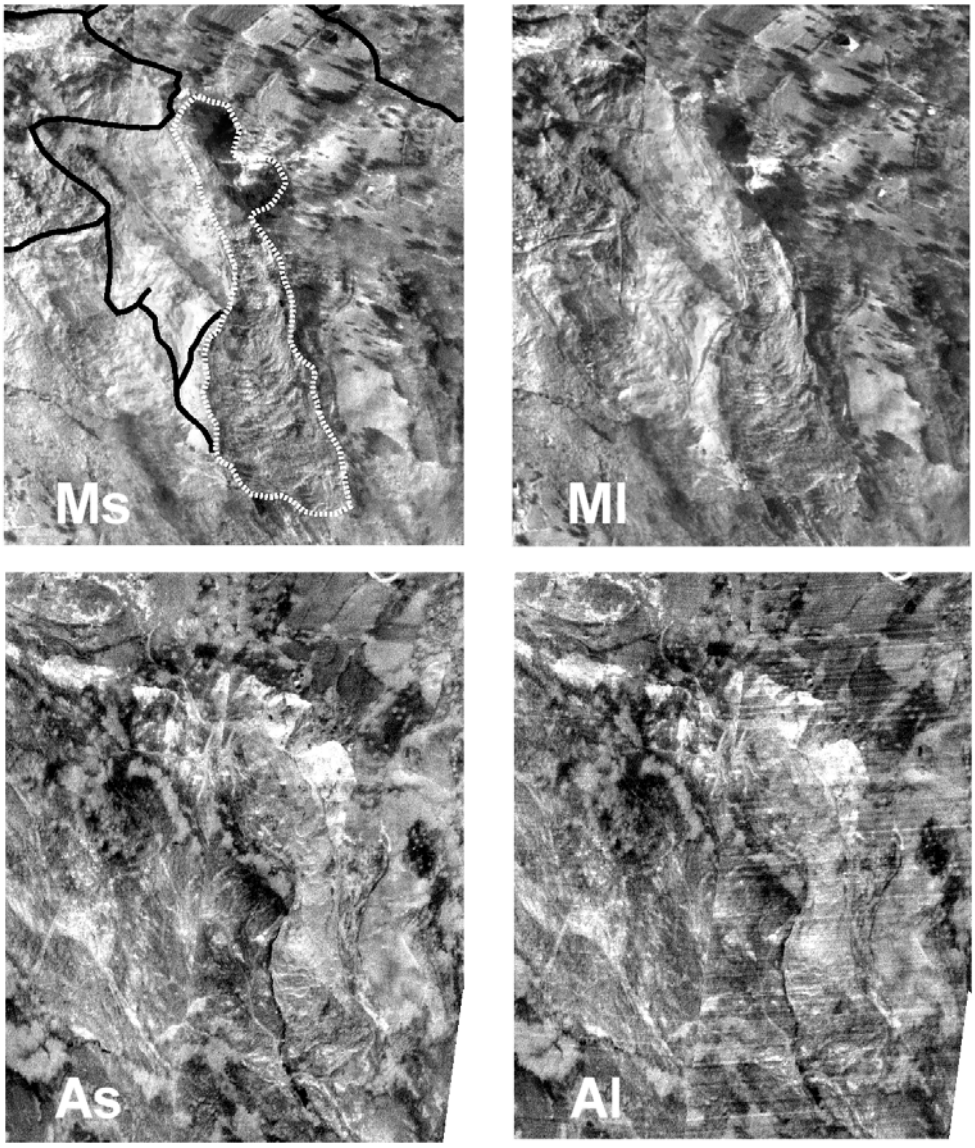

Fig.5. 1995 thermal infra-red images of the study area geometrically corrected and linearly stretched. “M” or “A” stand for morning or afternoon images, “s” or “l” for *short or long wave image*s. The white line is the SE2 landslide body whereas black lines represent the main roads.

often humid areas.

Fig. 5 helps identify the areas where surface water concentrates. Starting about halfway down the landslide body, along both sides of the earthflow, water pools along two linear paths and within some confined areas. The phenomenon, which is made evident by the minimum radiant energy, is clearly visible in the afternoon images on both sides and especially along the right one's (dark areas in Fig. 5). On-site surveys have confirmed it is a run-off which is partially fed by groundwater flowing from the saturated and non-saturated zone of the landslide body. The underground flow is probably almost orthogonal to the earthflow. On the right side, IR images have identified a runoff pooling fed by spring no. 4 (Fig. 3) located upstream. The spring water is evident in the As and Al images. The coolest areas proved to be pounding water resulting from the landslide counter-slope and spring water.

In the Ms and Ml images, the dark areas below the main scarp and on the left side of the same are not attributable to the high soil moisture but to the morphological effect of the shadowing of this area. The dark area absence in the afternoon images is a confirmation.

If morning images show a rather uniform landslide body, afternoon images highlight some white areas, which correspond to wide blocks of calcareous breccia as the one on the left of the main scarp (Fig.5).

Other geometric elements have been pointed out in different data processing images, obtained performing simple operations (as summa, product and difference) between the IR bands. For brevity, in this work only one example of this kind of operation has been presented in Fig.3B. Fig.3B has been obtained using the morning images combined in a *normalised difference ratio* (NDR). Each pixel of the image has been obtained as follows:

$$NDR = \text{sqrt}((Ms - Ml) / (Ms + Ml)) + 0.5 \qquad (I)$$

In this image, data elaboration highlights a change of tone and texture along the landslide body (marked by a dotted white line). Interestingly, this line runs parallel to that which marks a separation between the areas with different displacement rate represented in Fig.3A.

5. Conclusions

The integration of multidisciplinary long duration monitoring data by means of remotely sensed data carried out in this work yielded fruitful results. The main hydrogeological pattern, the geological and geomorphological framework and the areas of latent instability are determined. The relative rapidity by which this approach can be performed emphasises its usefulness.

The synoptic slope view contributes to an improved knowledge of complex phenomena as the one illustrated in this case study. The computer data-base can be easily upgraded with new data, especially after the landslide activity phases. Hence, the proposed approach can be regarded as a helpful contribution to the landslide hazard evaluation, particularly during emergency periods.

Acknowledgements. The authors thank the European Community – Environment Programme, for supporting the research in 1994-1996, as well as the Co-ordinator of the Research Project Prof. V. Cotecchia

References

Agnesi, V., Carrara, A., Macaluso, T., Monteleone, S., Pipitone, G., and Sorriso Valvo, M. (1983). Elementi tipologici e morfologici dei fenomeni di instabilità dei versanti indotti dal sisma del 1980 (Alta valle del Sele). *Geol. Appl. e Idrogeol.*, 18 (1), 309-341, Bari, Italy.

Alexander, D. and Coppola, L. (1989). Structural geology and the dissection of alluvial fan sediments by mass movements: an example from the southern Italian Apennines. *Geomorphology*, *2*, 341-361.

AMS (1999). CEO Algorithms, Models and Software Inventory: Tutorial Guide. *http:/ms.ceo.sai.jrc.it.8080/ams/tutorials/index.html*.

Celico, P. and Civita, V. (1976). Sulla tettonica del massiccio del Cervialto (Campania) e le implicazioni idrogeologiche ad esso connesse. *Boll. Soc. Nat. in Napoli*, Napoli, Italy, 85, 555-580.

Cotecchia, V. (1986). Ground deformations and slope instability produced by the earthquake of 23 November 1980 in Campania and Basilicata. *Geol. Appl. Idrogeol., 21* (5), 31-100, Bari, Italy.

Cotecchia, V., Del Prete, M., and Tafuni, N. (1986). Effects of earthquake of 23th November 1980 on pre-existing landslides in the Senerchia area (Southern Italy). *Geol. Appl. Idrogeol., 21*, 177-198, Bari, Italy.

Cruden, D.M. and Varnes, D.J. (1996). Landslide types and processes. In: Turner, A.K. and Schuster, L. (ed.*), Landslides. Investigation and mitigation*. Transportation Research Board, Special Report 247, Washington D.C., 36-75.

Del Gaudio, V., Calcagnile, G., Calvaruso, A. Pierri, P., and Trizzino, R. (1997). Attività sismica e franosità: il caso della frana di Serra dell'Aacquara (Senerchia, Av). Atti XVI Incontro Nazionale del Gruppo Nazionale di Geofisica della Terra Solida, CNR, Roma.

Drury, S. A. (1987). *Image interpretation in Geology*. Allen and Unwin. London.

EC (1996). Landslide evolution controlled by climatic factors in a seismic area. Prediction methods and warning criteria. Project coordinator: Prof. Cotecchia, V..

Guerricchio, A. and Melidoro, G. (1981). Movimenti di massa pseudo-tettonici nell'Appennino dell'Italia meridionale. *Geologia Applicata e Idrogeologia*, *16*, 251-294.

Lillesand, T.M. and Kiefer, R.W. (1994). *Remote sensing and image interpretation*. John Wiley and Sons. NY.

Maugeri, M., Motta, E., and Sorriso Valvo, M. (1982). The Senerchia landslide triggered by the November 1980 earthquake. Proc. IV Congr. IAEG, 8, 139-149.

Polemio, M. (1997). Rainfall and Senerchia landslides (Southern Italy). ABMS-ISSMFE, 2nd Panamerican Symposium on Landslides, Rio de Janeiro, 10-14 November 1997, I, 175-184.

Polemio, M. and Dragone, V. (1998). The role of climate in promoting landslides in the seismic area of the Appennines, Southern Italy). Proc. Int. Conf. on "Hydrology in a changing environment", British Hydrological Society, Exeter, 6-10 July, 1998, United Kingdom, John Wiley and Sons, III, 217-228.

Sabins, P.F. Jr. (1987). *Remote sensing, Principles and interpretation*. II ed. W.H. Freeman and Co., NY.

Santaloia, F., Cotecchia, F., and Polemio, M. (in press). Mechanics of a tectonized soil slope: influence of boundary conditions and rainfall. *Q.J. of Eng. Geol.*.

Thornthwaite, C.W. and Mather, J.R. (1957). *Instructions and tables for computing potential evapotraspiration and the water balance*. Pubbl. Clim. Drexel Inst. Technol., 10, 1-323.

Walsh, S.J., Butler, D.R., and Malanson, G. (1998). An overview of scale, pattern, process relationships in geomorphology: a remote sensing and GIS perspective. *Geomorphology*, *21*, 183-205.